Molecular Catalysis 533 (2022) 112749

Contents lists available at ScienceDirect

Molecular Catalysis

journal homepage: www.journals.elsevier.com/molecular-catalysis

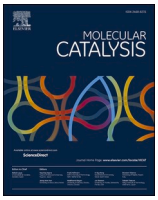

Mechanistic insight into the CO oxidation reaction at pure, Nb-doped and Mo-doped medium size Pt clusters

L.M. Molina *, C. Arranz-Simón, J.A. Alonso

Departamento de Física Teórica, Atómica y Optica, Universidad de Valladolid, E-47011 Valladolid, Spain

ARTICLE INFO

Keywords:
Clusters
DFT Calculations
CO Oxidation
Bimetallic catalyst
Heterogeneous catalysis

ABSTRACT

Density Functional Theory (DFT) simulations have been performed to study the CO oxidation reaction on a pure Pt_{18} cluster, and on Nb- and Mo-doped $NbPt_{17}$ and $MoPt_{17}$ clusters. The results show that a specially stable conformation of the pure cluster causes a sizable reduction of CO adsorption energy. Substituting one Pt atom by Nb or Mo has noticeable effects, charge transfer to the surface Pt atoms and destabilization of the special Pt_{18} ground state conformation, which result in an enhacement of CO binding for the doped cluster. Finally, molecular oxygen binds strongly to pure and Nb- or Mo-doped clusters, and easily dissociates and reacts with co-adsorbed CO, with reaction barriers not exceeding 0.8 eV.

1. Introduction

Platinum nanocatalysts have multiple applications. To name a few, these nanocatalysts are widely used in proton exchange membrane fuel cells (PEM-FCs) [1,2], and are relevant to oxygen reduction, hydrogen oxidation, and hydrogen evolution reactions [3]. The high catalytic activity for the decomposition of hydrogen peroxide suggest the use of Pt nanoparticles as antioxidants against oxidative chemical compounds [4]. The application of platinum catalysts for the high-yield oxidation of methane to metanol has also been reported [5]. It is well know that particle size has a critical impact on the performance of the catalysts [6], and new and unique effects appear in the subnanometer region, when the particle size is reduced up to a few atoms [7,8]. For a number of reactions involving oxidation, unexpected catalytic properties are observed at extremely small sizes [9–17]. In these systems, both the electronic structure and the geometrical features vary in very complex ways with cluster size, and are quite different from either bulk Pt or large nanoparticles with fcc packing [18–22]. For potential practical uses in various oxidation reactions, one of the issues most widely studied is the susceptibility to carbon monoxide poisoning [23] (that is, the accumulation of CO on most of the active sites of the Pt particle making impossible adsorption of other relevant reactants). This gas is usually present in trace amounts as a contaminant element in many fuels, and it is extremely important to develop new catalysts with improved resistance to CO poisoning.

One of the most promising ways of overcoming these problems is by doping the Pt catalysts with small quantities of other transition metals. While for large particles, the mechanisms behind a weakening of the Pt-CO bond by adding impurities have been extensively studied [24,25], the influence of dopants on the catalytic properties of small Pt_N clusters is poorly understood. Recently, experiments on CO reactivity of Pt_N clusters (N=13-23), both pure and doped with various 4d elements [26,27], have shown that the presence of some impurities (Mo, Nb) causes a sizable drop in CO binding energy to the cluster. In these clusters, the origin of such enhanced tolerance towards CO poisoning seems to be related to a sizable charge transfer from the dopant to the Pt atoms, which produces important changes in the electronic structure of the cluster. Doping the Pt nanoparticles with germanium also provides an effective way to mitigate CO poisoniong [28].

These results have motivated us to analyze the mechanisms for CO removal on these clusters, during oxidation reactions, by studing in detail the CO oxidation reaction to CO_2 in platinum clusters doped with Nb or Mo. This reaction has been intensively studied for many small clusters of various transition metals [29,30], with the results showing drastic changes of reactivity with cluster size [31,32]. In particular, the catalytic oxidation of CO on Pt systems has been investigated in several works. Different reaction conditions have been tested on solid Pt surfaces [33–35] and theoretical calculations have been performed as well [36]. In the case of pure platinum clusters, Heiz et al. [37] have found a sharp increase in reactivity for Pt_N clusters with more than 15 atoms. Beniya et al. have also found large activity variations for Pt_N clusters in the rage N=10-20 [38]. Vendelbo et al. [39] noticed periodic changes in

* Corresponding author.
E-mail address: lmolina@fta.uva.es (L.M. Molina).

https://doi.org/10.1016/j.mcat.2022.112749
Received 2 April 2022; Received in revised form 26 September 2022; Accepted 13 October 2022
Available online 27 October 2022

the CO oxidation rate on unsupported Pt nanoparticles, and demonstrated that this oscillatory behavior is correlated to the dynamical periodic refacetting of the nanoparticles. Different experimental techniques have been employed to analyze the oxidation of CO on supported Pt nanoprticles [40–42]. Single-atom catalytic oxidation of CO has also been investigated. Feng et al. [43] studied Pt single-atom catalytic oxidation of CO for Pt adsorbed on CeO_2 and Pt adsorbed on Ga-doped CeO_2. Different mechanisms were observed in the two systems, and vacancies formed near the Ga impurities were found to play an important role in activating the oxygen molecule. Work on Pt nanoalloys is scarce. Lian et al. [44] have performed DFT simulations to study the CO oxidation reaction in mixed Pt_3M clusters (M = Pt, Ni, Mo, Ru, Pd, Rh), finding strong differences in the activation barriers for different dopants.

To gain additional insight into the changes induced by the presence of an impurity in the CO oxidation activity of small Pt_N clusters, we have studied in detail all the steps of the reaction in both a pure and a Nb-doped Pt_{18} cluster. Also, we have tested with some additional simulations the effect on the reaction of changing the dopant to Mo, another impurity which has been observed to affect the CO binding energies. We have chosen such cluster size for several reasons; first, previous theoretical studies have focussed on either very small Pt_N clusters [45–49] or large nm-sized Pt nanoparticles [50]. Second, this cluster size (around 20 atoms) coincides with both the large increase in reactivity observed by Heiz et al. [37] for pure Pt clusters, and with the size range where Ferrari et al. [26] have found a larger influence of the presence of Nb on the binding of CO to the cluster. Finally, as it will be discussed later, the Pt_{18} cluster has some interesting properties, as an intrinsically high stability due to a magic triangular prism shape, which has an important influence on the reactivity of this cluster towards CO binding. We will show that oxidation of CO to CO_2 by coadsorbed O_2 on Pt_{18} and $NbPt_{17}$, and the elimination of CO_2 are relatively easy due to the strongly favourable reaction energies and moderate activation barriers for these processes.

2. Computational setup

Density Functional Theory (DFT) calculations were carried out using the projector augmented-wave method, as implemented in the GPAW code [51,52]. Each cluster was placed at the center of a large cubic cell (18 Å × 18 Å × 18 Å) with the spacing of the real-space three-dimensional grid set to 0.2 Å. Convergency tests with cubic cells of sizes up to 25 Å were performed (see the table T1 in the supplementary material), showing that at 18 Å the binding energies of CO and O_2 to the cluster are converged with a precision of approximately 0.01 eV. Exchange-correlation effects were modelled with the PBE functional [53,54]. The pseudopotentials for Pt, Nb, C and O included, respectively, 10, 5, 6 and 8 valence electrons. In the case of Pt, the pseudopotential includes scalar-relativistic effects. Spin-polarized calculations were carried out for all species, to take into account magnetization of the Pt atoms. As it will discussed later, the absorption of either CO or O_2 species can affect the magnetization state of the cluster in quite complex ways. The convergence threshold for the eigenstate energies was set to $5{\cdot}10^{-7}$ eV/e^-. Structure optimization was carried out using the BFGS (Quasi--Newton) algorithm [55] until forces on the atoms were below 0.01 eV/Å.

Energy barriers were calculated by a constrained minimization method, involving several simulations where the reaction coordinate (either O-O or C-O distances) was restricted at increasingly smaller values, while allowing the rest of the system to freely relax [36]. Transition structures were characterized as energy maxima in the reaction profile, testing various candidate conformations for the critical value of the reaction coordinate, until the barrier height was obtained with at least a precision of 0.05 eV.

3. Results

3.1. CO adsorption at Pt_{18} and $NbPt_{17}$

Prior to the catalysis study, we have performed an extensive isomer search to identify the most stable conformation for both Pt_{18} and $NbPt_{17}$. The most stable structures are shown in Fig. 1. In the supplementary material (Figures S1, S2, S3 and S4), the equilibrium structures for other alternative conformations, as well as their relative energies, are shown. In this isomer search, we prepared a large number of diverse candidate structures, studing almost every possible reasonable packing type of the atoms within the cluster (icosahedral, simple cubic, face-centered cubic, and combinations of those). For Pt_{18}, in agreement with previous studies by Kumar et al. [18], the most stable conformation is a triple stack of equilateral Pt_6 triangular subunits (Fig. 1a). Interestingly, our isomer search shows that such triangular conformation is a very stable and "magical" shape, as any other competing conformation lies more than 1 eV higher in energy. This fact simplifies a lot the isomer search in the case of the pure cluster. Among the other isomers, we have selected a conformation based on two stacked rectangular Pt_9 units (Fig. 1b) for performing additional simulations of the binding of CO, to check the effect of cluster structural features and spin on reactivity. It is interesting to observe that for a fixed cluster size, varying the type of atomic packing and symmetry results on huge variations of the total magnetic moment, which decreases from $8\mu_B$ to $0–1\mu_B$.

In the case of $NbPt_{17}$, the isomer search becomes a problem much more complex, which involved both testing the most stable isomers for Pt_{18}, with one Pt atom substituted by Nb, and also many other uniquely new conformations. Interestingly, the results in Figures S2, S3 and S4 show that the simple substitution of Pt by Nb on the triple stacked triangle (conformer 13) in Fig. S3) leads to a not very stable structure. In general, there is a strong tendency for the Nb atom to be located at the center of the cluster, and any atempt to move the impurity towards the surface has a high energetic cost (as the results for isomers 25, 26 and 27 in Figure S4 show). This effect has been previously reported by Ferrari et al. [26] for a series of 4d impurities (Mo, Nb, etc...) on platinum clusters of medium sizes. When we restrict the isomer search to conformations with a central Nb atom, the number of candidate structures to explore is drastically reduced, and it is now much probable to locate a conformation which can be the true global minimum. As lowest energy structures of $NbPt_{17}$, we found 2 almost degenerate conformations (with a difference in total energy less than 0.01 eV), shown in Fig. S2 as conformers 1) and 2). The former (structure S2-1) is actually a transformation of the triple stacked triangle, with the central triangle distorted (expanded) in order to accomodate a Nb atom at the center. The latter (structure S2-2), is an octahedral structure, also with a Nb atom at its center, and with one of the edge Pt atoms missing. For the catalysis studies, we decided to choose isomer S2-1) (the one shown in Fig. 1c), as it is the conformation which has more structural similarities with the triangular structure of pure Pt_{18} and it is more likely to be produced in experiments.

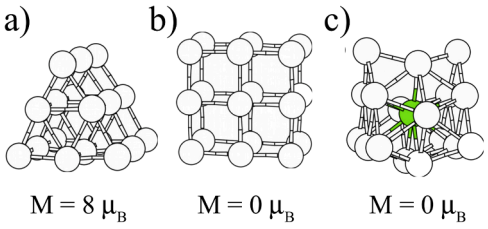

Fig. 1. Equilibrium structures and magnetic moments of Pt_{18} (in two different conformations; the most stable one is structure a) and $NbPt_{17}$ clusters. The Nb impurity in represented by a green sphere. (For interpretation of the references to colour in this figure legend, the reader is referred to the web version of this article.)

Next, we have performed an extensive investigation of the adsorption of CO on every cluster under study, considering every inequivalent binding site. Fig. 2 shows the CO binding energies at Pt_{18}, calculated using the formula:

$$E_b(CO) = E(CO) + E(Pt_{18}) - E(CO/Pt_{18}) \quad (1)$$

For this cluster we have studied CO adsorption at both the stacked triangles (upper panel of Fig. 2) and the stacked squared conformations (lower panel of Fig. 2). In the first case, we find that conformer a) is the most stable adsorption site for CO, with the carbon monoxide molecule bridging two Pt atoms at one side of the triangular prism. This configuration is only 0.05 eV more stable than conformer b), with CO slightly displaced to a location on top of a Pt atom at the edge of the prism. At other alternative binding sites (conformers c-f) the CO binding energy is even lower (around 1.5 eV or less). This means that coadsorption of several CO molecules will become increasingly less favoured, and the cluster is therefore more resistant to poisoning by CO. The bridge and on-top adsorption positions of CO are in agreement with the results of the X-ray Photoelectron Spectroscopy (XPS) [56], and Infrared Reflection Absorption Spectroscopy (IRAS) analysis [57] of the adsorption of CO on Pt(110) surfaces, and vibrational spectroscopy analysis of the adsorption of CO on Pt(111) surfaces [58,59].

It is important to comment on the relatively low value of the CO binding energy (1.77 eV) for this cluster. In a previous study [26], we found for pure cationic Pt clusters of comparable size (Pt_{19}^+) much higher CO binding energies, of the order of 2.4 eV. Apparently, the overall high intrinsic stability of this Pt_{18} isomer (much more stable than any other conformation, and perhaps related to its high spin state) causes a significant drop in CO binding energy. In the figures, we report the value of the cluster's magnetic moment after CO binding. In the case of the triangular prism isomer, CO adsorption at every binding site causes a decrease from $8\mu_B$ (the magnetic moment of the clean cluster) to $5–6\mu_B$. The results for the stacked squared conformation (lower panel of Fig. 2) show a higher CO binding energy for this isomer (2.04 eV). This confirms the fact that the relatively low reactivity of the triangular prism isomer is strongly linked to its special shape, and as soon as we depart from that shape reactivity rises.

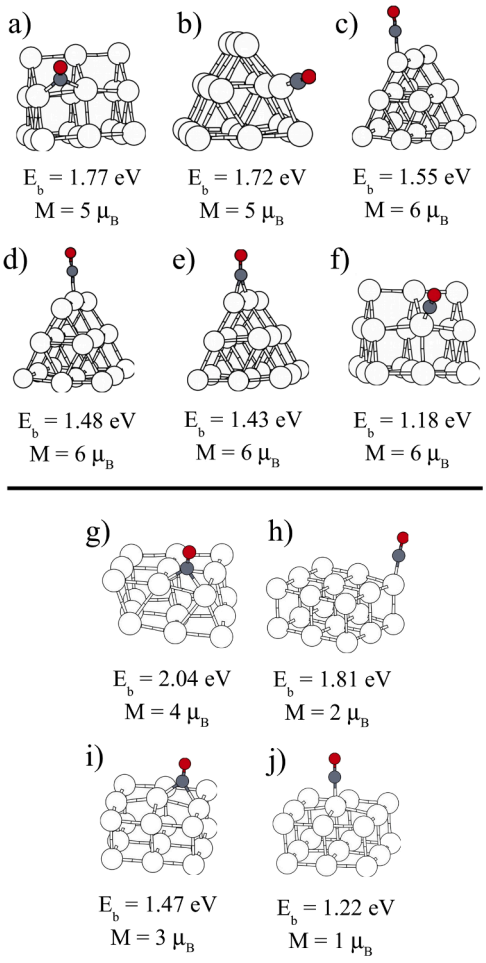

Fig. 2. Equilibrium structures, binding energies and magnetic moments for CO adsorption at a Pt_{18} cluster. The upper panel shows conformations of CO at a triangular prism isomer, and the lower panel configurations of CO adsorbed at an stacked square isomer. White, gray and red spheres represent Pt, C and O atoms, respectively. (For interpretation of the references to colour in this figure legend, the reader is referred to the web version of this article.)

Now we analyze in detail the effect caused by CO adsorption on the magnetism of the platinum cluster. In general, binding of CO (and, as we will see later, other molecules as well) results in a marked decrease of the local magnetic moment at the host Pt atoms. In panels a) and b) of Fig. 3, we have respectively plotted the local spin density (difference between electron density components with up and down spins) for both bare triangular Pt_{18} and for CO adsorbed to this cluster in its more stable conformation. Two facts are worth noticing: first, the spin density is in general quite uniformly distributed over all the atoms (corners, edges, etc.) of the Pt_{18} cluster. Second, the presence of CO results in a marked drop of spin density at the host Pt sites. As a result of this drop, the overall magnetization of the cluster decreases from $8\mu_B$ to $5–6\mu_B$. This effect of decreasing magnetization at the CO binding host sites does not always lead to the trivial result of an overall cluster magnetization drop; in the case of the stacked square isomer of Pt_{18}, we found a very interesting exception. Panel c) of Fig. 3 shows the spin density of this squared conformation with CO adsorbed. Although the magnetization at the host Pt sites is also low, for this conformation we found that CO adsorption results in a marked increase of the total magnetization of the cluster, which rises from 0 to $4\mu_B$.

To gain additional insight into the features of CO binding to these clusters, we have also analyzed the densities of electronic states (DOS). Fig. 4 shows the spin-polarized DOS for Pt_{18} with triangular prism conformation (first panel), Pt_{18} with stacked square confirmation (second panel) and for the most stable conformation of CO bonded to Pt_{18} with either triangular prism (third panel) or stacked square shape (fourth panel). For the bare cluster (with either triangular or square conformation) the almost full d-band has a relatively high DOS around the Fermi level. For the triangular conformer, those frontier orbitals split into two contributions, with spin up just below the Fermi level (and therefore occupied) and another one with spin down just above the Fermi level, giving rise to the large magnetic moment of the cluster. A small 0.12 eV gap opens at the Fermi level, a feature which causes the cluster to become more stable and less reactive. In the case of the square conformation, both spin up and down contributions lie just below the Fermi level, with a null total spin. Adsorption of CO to this square conformer results in a symmetry break-up, and Jahn-Teller effects are then largely responsible for the displacement of some spin-down states above the Fermi level and the associated final net magnetic moment of the cluster with CO adsorbed. On the other hand, the third panel of Fig. 4 shows that adsorption of CO on the Pt_{18} triangular prism structure induces the shift of some spin up states from below to above the Fermi energy, with the ensuing lowering of the magnetic moment. In this figure, we have also plotted the projection of the DOS into the CO molecular orbitals, as well as three dimensional plots of the CO-Pt_{18} hybrid orbitals. Comparison with the molecular orbitals of free CO indicates that the 5σ orbital is strongly shifted down in energy, with a quite sizable degree of hybridization with the d orbitals of the two host Pt atoms.

The results for CO adsorption at various binding sites on the most stable $NbPt_{17}$ cluster are shown in Fig. 5. The most stable conformation corresponds to CO bonded to one of the Pt atoms in the central atomic plane (the one which contains Nb and six Pt atoms almost surrounding

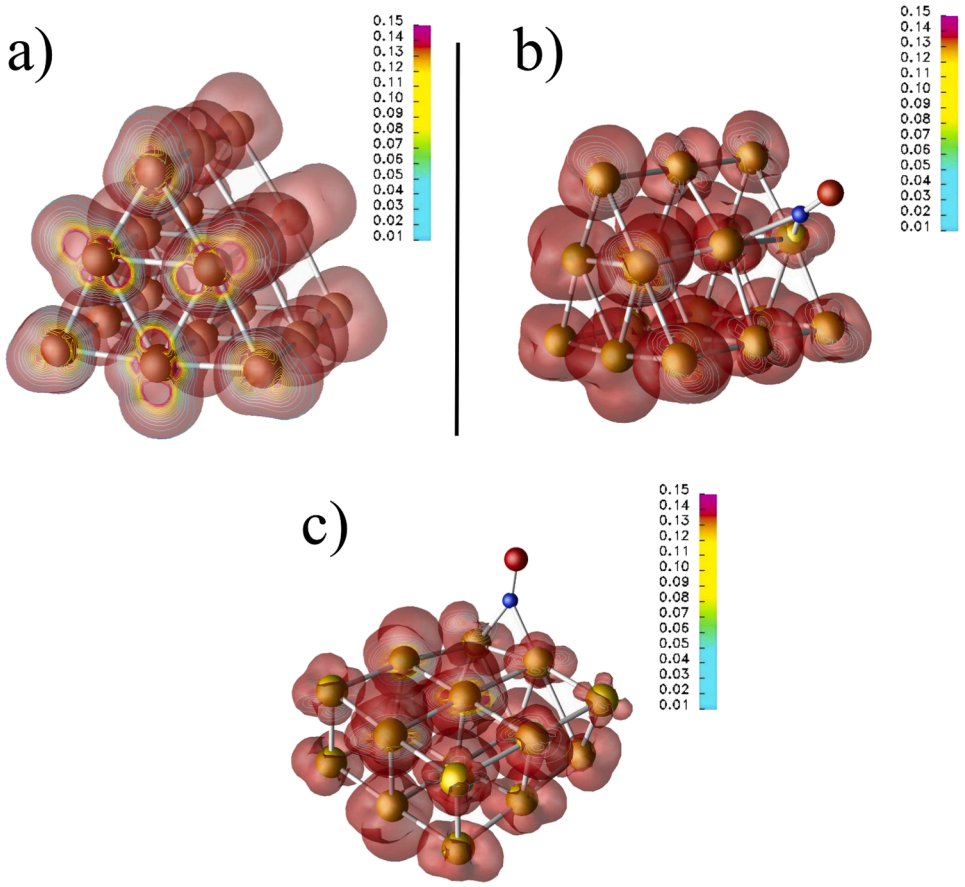

Fig. 3. Spin density plots for a) Clean Pt_{18} (triangular prism isomer), b) CO adsorbed on the triangular prism isomer of Pt_{18} and c) CO adsorbed on the stacked square isomer of Pt_{18}. The red three-dimensional contours plot a constant value of 0.01 $e^{-}/Å^3$. Superimposed, coloured curves (values given in color bar at one side) show cuts of equal spin density on a plane which cuts through the centers of the Pt atoms on a cluster's face. (For interpretation of the references to colour in this figure legend, the reader is referred to the web version of this article.)

it), with a rather high (2.05 eV) binding energy. Other stable conformations, (b) and (c), have also quite high binding energies, close to 2 eV. Comparing these binding strenghts with the highest CO binding energy for CO at triangular prism Pt_{18} (less than 1.8 eV) it becomes clear that the effect of Nb doping is to increase the strength of CO-Pt bonds. This occurs because the insertion of the Nb atom in the interior of the Pt cluster distorts substantially the very stable triangular prismatic structure, producing a structure less symmetric and more reactive. Finally, it is worth noticing that the least stable conformation in Fig. 5 corresponds to CO bonded to three Pt atoms. Such "hollow" adsorption sites are strongly disfavoured against more stable conformations with CO on top of Pt atoms or bridging two Pt sites.

As in the case of pure Pt_{18}, we have plotted in Fig. 6 the DOS for both clean $NbPt_{17}$ and the cluster with a CO molecule adsorbed. In the plots we show the projection of DOS onto the Nb d orbitals and onto the CO molecular orbitals. In both cases, a part of the Nb orbitals are located around -3 eV (well above the Fermi level) and the rest of the Nb orbitals are strongly hybridized with the Pt orbitals. This means that a substantial part of the Nb electronic charge is transferred to the platinum d-band. From the total electronic density, we have calculated the Bader charges [60], obtaining net positive charges on the Nb atom for $NbPt_{17}$ and CO-$NbPt_{17}$; specifically, the Nb atoms have a deficit of 1.73 and 1.71 electrons, respectively (see Figure S5 in the supplementary material). The transferred charge is distributed more or less uniformly on the surface Pt atoms, with each of them gaining about 0.10 electrons. The charge transfer from Nb to the Pt d-band results on a larger degree of filling of this band. The analysis of the hybridized CO-Pt states show some differences with respect to the results for pure Pt_{18}. First, the two 1π levels are degenerate (instead of being split in two as for Pt_{18}), a fact that can be attributed to the different type of coordination (on top of Pt for $NbPt_{17}$, and with CO bridging to Pt atoms for Pt_{18}). Second, and more important, the separation between the 4σ and 5σ states is smaller in CO-$NbPt_{17}$ as compared to CO-Pt_{18} (2.33 eV versus 3.20 eV).

3.2. O_2 adsorption at Pt_{18} and $NbPt_{17}$

For the CO oxidation reaction, another key step is the adsorption (and subsequent dissociation) of molecular oxygen at the clusters. In the same way as for CO, we have performed an extensive study of the stability of the O_2 molecule adsorbed at various sites of either Pt_{18} or $NbPt_{17}$. The results are shown in Fig. 7. In all cases, O_2 has a strong preference towards conformations bridging two Pt atoms. For Pt_{18}, the most stable adsorption site involves two Pt atoms along a lateral edge of the triangular prism, which agrees with the predictions from the calculations of Wang et al. [61] At this location, O_2 binds quite strongly, with more than 1.5 eV binding energy. Interestingly, displacing the molecule to other conformations on faces around the cluster results in a sharp decrease of its stability, by amounts between 0.5 and 1 eV. As it happened in the case of CO, adsorption of molecular oxygen leads to a sizable decrease in the magnetization of the cluster, from $8\mu_B$ up to $4–6\mu_B$.

When O_2 is bonded to Pt_{18} at its more stable conformation, the O-O bond length expands to 1.40 Å (with respect to a value of 1.23 Å for gas-phase O_2). Previous DFT simulations of O_2 adsorption at other transition metal clusters [61,62] indicate that values of O-O bond lengths around 1.32 Å are characteristic of oxygen binding in a superoxo O_2^- electronic state, whereas expansion of O-O bond length up to 1.40-1.45 Å indicate adsorption of O_2 in a peroxo O_2^{-2} electronic state. Our computed value of 1.40 Å then suggests that the oxygen molecule can attain a peroxo state when binding to Pt_{18}. The upper panel of Fig. 8 (where we show the total and O_2-projected DOS for the O_2-Pt_{18} complex) further confirms this fact. After adsorption, the oxygen $1\pi^*$ antibonding states (strongly

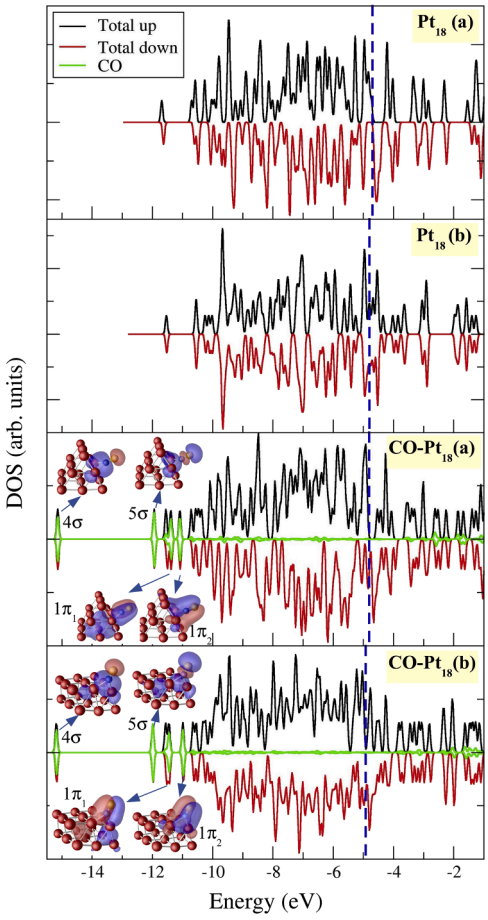

Fig. 4. Spin-polarized densities of electronic states (DOS) for clean Pt_{18} with triangular prism shape (first panel), clean Pt_{18} with stacked square shape (second panel), CO adsorbed to Pt_{18} with triangular prism shape (third panel) and CO adsorbed to Pt_{18} with stacked square shape (fourth panel). Black and red lines represent, respectively, spin up and down contributions to the DOS. Dashed blue lines show the position of the Fermi energy. In the case of CO andsorbed to Pt_{18}, green lines show the projection of the DOS into carbon and oxygen s and p atomic orbitals. Insets show three-dimensional shapes of some of the mixed CO-cluster molecular orbitals. (For interpretation of the references to colour in this figure legend, the reader is referred to the web version of this article.)

hybridized to Pt d states) are almost completely filled, indicating an almost complete peroxo O_2^{-2} state. The analysis of Bader charges (see data in Figure S5 of supplementary material) indicates the gain of around 0.3 electrons by each of the oxygen atoms of O_2. Such charge is transferred mostly by the two Pt atoms bonded to the oxygen molecule.

In the case of $NbPt_{17}$, O_2 also binds quite strongly, with a maximum binding energy of 1.42 eV. This value is only 0.15 eV smaller than the corresponding one for Pt_{18}, meaning that the tendency towards oxidation is not greatly affected by the presence of the impurity. For the configuration in Fig. 7e, the O-O bond distance is 1.41 Å, meaning again that the adsorbed oxygen molecule is in a peroxo electronic state. This is further confirmed by the analysis of the DOS shown in the lower panel of Fig. 8, with very similar features to the case of O_2 adsorbed on Pt_{18}; both the binding energy of each oxygen orbital and their degree of hybridization with Pt d states. Also, examining the various values of the binding energies at different sites, we find again an important variability of around 0.5-1 eV. Finally, the calculated Bader charges show a very similar extra charge to be present in the adsorbed O_2 molecule. A close examination of charges around the O_2-$NbPt_{17}$ complex shows that charge to O_2 is also mainly donated by the Pt atoms bonded to O_2 and, quite surprisingly, the positive charge on the Nb impurity is not modified at all after oxygen adsorption.

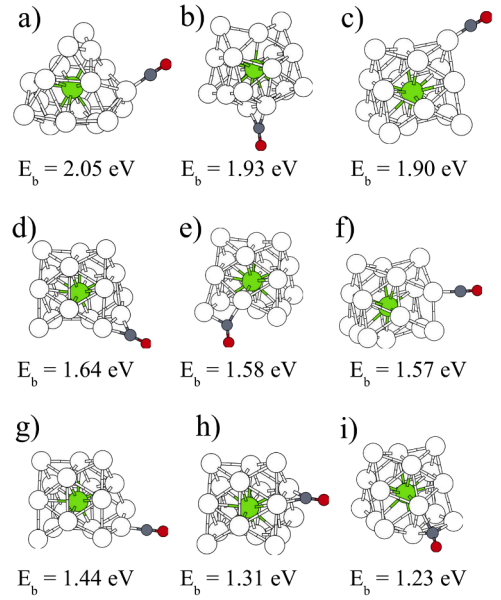

Fig. 5. Equilibrium structures and binding energies for CO adsorption at a $NbPt_{17}$ cluster. In all cases, the magnetic moment is zero. The green sphere represent the Nb atom. (For interpretation of the references to colour in this figure legend, the reader is referred to the web version of this article.)

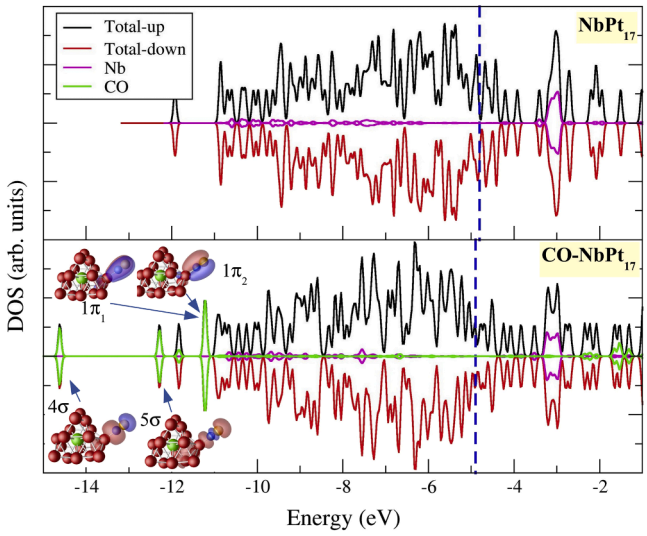

Fig. 6. Spin-polarized densities of electronic states (DOS) for clean $NbPt_{17}$ and CO adsorbed to $NbPt_{17}$. Magenta and green lines show partial projections of the DOS into Nb and CO orbitals, respectively. Insets show 3D shapes of some of the mixed CO-cluster molecular orbitals. (For interpretation of the references to colour in this figure legend, the reader is referred to the web version of this article.)

3.3. *CO and O_2 coadsorption at Pt_{18} and $NbPt_{17}$*

Before studying reaction pathways and energy barriers for CO_2 formation at these clusters, we have performed extensive simulations of the CO and O_2 molecules co-adsorbed around each of the clusters under study, in order to determine the most stable initial states for the reaction. In the case of Pt_{18}, Fig. 9 shows the relaxed structures, binding energies and magnetic moments for all the configurations studied. For the binding energy, we report on each case two quantities: first, the total

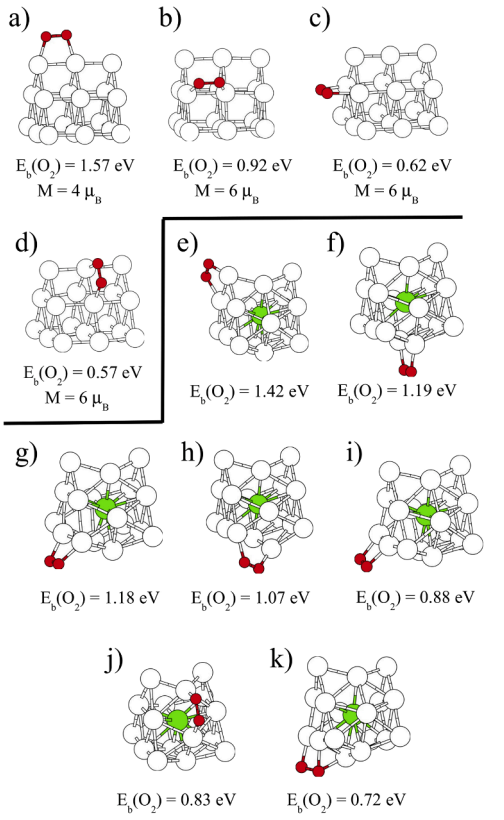

Fig. 7. Equilibrium structures and binding energies for O_2 adsorption at Pt_{18} and $NbPt_{17}$ clusters. In the case of O_2 adsorbed at $NbPt_{17}$, the magnetic moment is always zero.

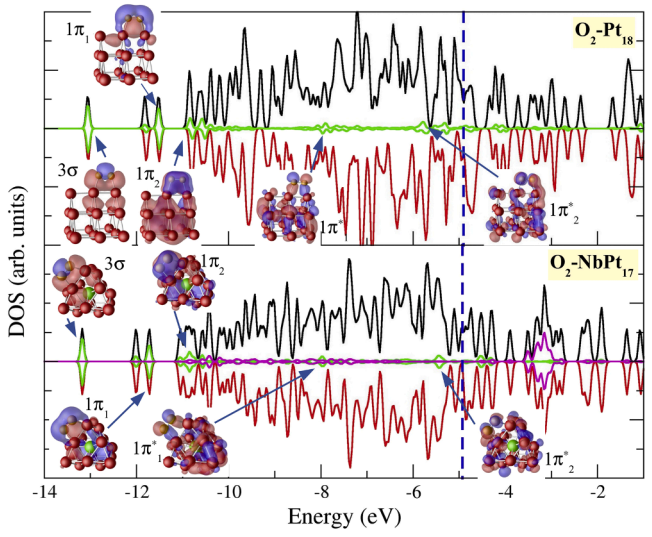

Fig. 8. Spin-polarized densities of electronic states (DOS) for O_2 adsorbed at Pt_{18} and $NbPt_{17}$ clusters. Magenta and green lines show partial projections of the DOS into Nb and O_2 orbitals, respectively. Insets show three-dimensional shapes of some of the mixed O_2-cluster molecular orbitals. (For interpretation of the references to colour in this figure legend, the reader is referred to the web version of this article.)

binding energy E_b(total), that is, the energy gain after the consecutive adsorption of CO and O_2, with respect to the clean cluster and both gas-phase molecules:

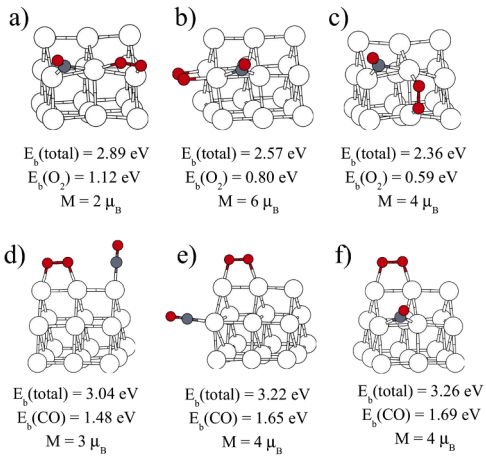

Fig. 9. Equilibrium structures, binding energies and magnetic moments for coadsorption of CO and O_2 at a Pt_{18} cluster.

$$E_b(\text{total}) = E(\text{CO}, g) + E(\text{O}_2, g) + E(\text{Pt}_{18}, g) - E(\text{CO/O}_2/\text{Pt}_{18})$$

Second, we report, depending on the conformation, $E_b(O_2)$ (the binding energy of O_2 with CO preadsorbed on the cluster), or E_b(CO) (the binding energy of CO with O_2 preadsorbed on the cluster).

In order to search for suitable starting points for the CO oxidation reaction, we have considered two types of conformations: first, with CO in its more stable binding site, and O_2 at various sites around the pre-adsorbed CO. Second, having O_2 located at its most stable site, we have relaxed several alternative positions of CO around the preadsorbed O_2. In the first case (conformations a, b, c, in Fig. 9) CO and O_2 bind in very close proximity, sharing one Pt atom. Interestingly, we find a sizable cooperative effect, as the O_2 binding energy with CO preadsorbed is higher than the corresponding binding energy in the absence of CO (at the same binding site). Cooperativity for coadsorption is highest for conformer (a), with an enhancement on O_2 binding of 0.20 eV. As it should be expected, the magnetic moment of the Pt_{18} cluster decreases (in a varying amount) upon succesive absorption of the CO and O_2 species. The second case (conformations d, e, f) represents more stable configurations, with total binding energies above 3 eV. For each of these, there is only a very small competitive effect (0.08 eV or less) upon CO and O_2 coadsorption, and the total binding energy is approximately equal to the sum of individual CO and O_2 adsorption energies. The most stable case (f) corresponds, of course, to the combination of the most stable conformations for either CO and O_2.

In Fig. 10, we show the results for CO and O_2 coadsorption at $NbPt_{17}$. As in the Pt_{18} case, we have focussed on two alternatives: first, placing CO on two of its more stable locations, with O_2 around it (conformations a-g). Second, placing O_2 on its more stable location, and co-adsorbing CO at various sites around the cluster (conformations h-k). In general, we find a similar behaviour as in the Pt_{18} case, with a very weak competivive effect for CO-O_2 coadsorption in most conformations, and some few cases with moderate cooperative effects; this is the case for conformer (j), which is also the most stable configuration, with a total binding energy of 3.56 eV.

3.4. CO oxidation reaction at Pt_{18} and $NbPt_{17}$

Finally, we discuss the reaction pathways and energy barriers for CO_2 formation from coadsorbed CO and O_2 on either of the two clusters under study. For each cluster, we have studied two alternate Langmuir-Hinshelwood reaction pathways, starting from different initial CO/O_2 coadsorption conformations. We have also performed some test simulations (see Figure S6 in the supplementary material) to check if an Eley-

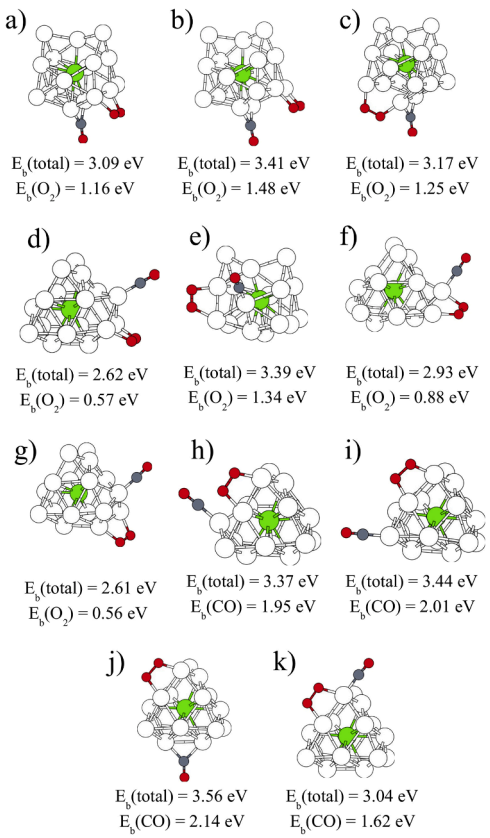

Fig. 10. Equilibrium structures, binding energies and magnetic moments for coadsorption of CO and O_2 at a $NbPt_{17}$ cluster.

Rideal mechanism can take place, with CO directly reacting from the gas phase with oxygen atoms preadsorbed at the cluster. It turns out that such pathway is completely unfeasible, as any approaching CO molecule will strongly prefer to bind to any available Pt site first, rather than form a bond with a preadsorbed O atom. The reason behind this behaviour lies on the high stability (above 1.5 eV) of the CO-Pt bonds. The results for the Langmuir-Hinshelwood reaction pathways at Pt_{18} are shown in Figs. 11 and 12. In the first case we have taken conformation (a) in Fig. 9 as the starting point for the reaction (with CO bonded at its more stable location, and O_2 located next to CO, sharing one Pt atom). The first step of the reaction involves dissociation of the adsorbed oxygen molecule into two adsorbed oxygen atoms placed at Pt-Pt bridge sites neighbour to the CO molecule. We obtain a moderate 0.81 eV energy barrier for this process, being this the limiting step of the whole reaction (that is, the one characterized by the highest barrier). The barrier maximum occurs at a distance of 2.0 Å in the elongated oxygen-oxygen bond (see inset labeled TS1 in Fig. 11). At this point, it is important to remember that an alternative pathway, involving direct reaction between CO and intact O_2, leading to formation of an adsorbed O-C-O-O complex, could perhaps compete with the pathway shown in Fig. 11 (for small clusters of other transition metals, as gold for example, this is actually the case [63,64]). In order to rule out such possibility, we have performed some test simulations for that process, finding that it can only take place by overcoming quite high energy barriers (well above 1 eV). Therefore, CO_2 formation must necessarily take place only after previous dissociation of O_2. Finally, it is interesting to compare the moderate barrier height for O-O dissociation to the large O_2-Pt_{18} binding energy (of the order of 1.5 eV). It is quite possible that, upon adsorption of O_2, the large release of thermal energy associated to the formation of the O-Pt bonds could lead to an spontaneous activation of the O-O bond and to the dissociation of O_2 inmmediately after its adsorption.

The intermediate state with dissociated O_2 is approximately 0.5 eV more stable than the initial state with adsorbed molecular O_2, meaning that there is a moderate tendency towards the partial oxidation of the surface of the Pt_{18} cluster. Then, the second reaction step involves diffussion of one of the adsorbed oxygen atoms which reacts with the neighbour CO. The height of this second barrier is smaller (0.43 eV) and its maximum occurs when the reacting oxygen is located at a distance of 1.9 Å from the C atom (see inset labeled TS2 in Fig. 11). After overcoming the barrier, the atoms relax towards a final conformation with the CO_2 molecule forming two bonds with Pt atoms in the cluster, and with the carbon atom in sp^2 hybridization, forming and angle of approximately 120° with the oxygen atoms. CO_2 formation is energetically favourable, and the overall binding energy of the adsorbed CO_2 (plus a coadsorbed oxygen adatom) with respect to gas-phase CO and O_2 is around 4 eV. This result is consistent with the work of Su and coworkers [58], who had earlier found that CO oxidation on the surface of the Pt metal is very exothermic.

The final reaction step involves desorption of CO_2 to the gas phase. This process takes place throught breaking of the O-Pt bond (see inset labelled TS3 in the figure), which only requires to overcome a small barrier of 0.28 eV. Once the TS is reached, relaxation of the structure produces a spontaneous breaking of the remaining C-Pt bond, and desorption of CO_2.

Next, we will consider an alternate pathway for the reaction, based

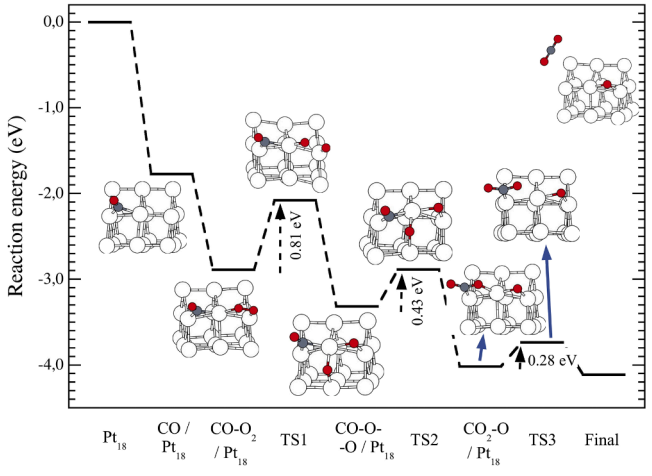

Fig. 11. Reaction energies and energy barriers for CO_2 formation at a Pt_{18} cluster (first pathway). Insets show the relaxed structures of all the intermediate and transition states.

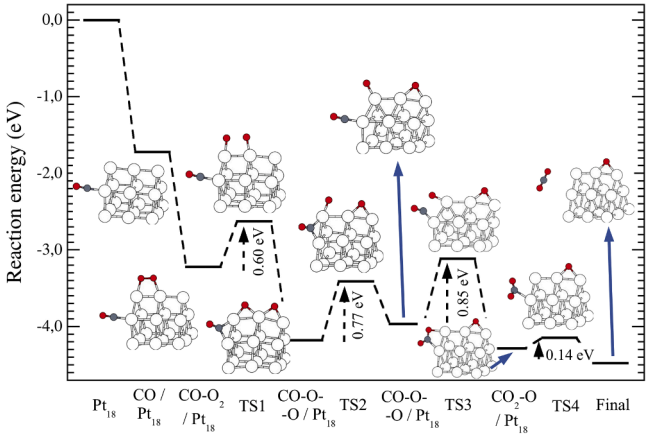

Fig. 12. Reaction energies and energy barriers for CO_2 formation at a Pt_{18} cluster (second pathway). Insets show the relaxed structures of all the intermediate and transition states.

on starting from a conformation with O_2 bonded at its most stable location, and CO placed nearby (see Fig. 12). As in the previous case, we have also performed some tests for the direct reaction between CO and intact O_2, again with negative results (barriers above 1 eV). This means that the reaction again must necessarily start with dissociation of O_2. This step is now slightly easier, with a barrier of 0.60 eV. After breaking of the O-O bond (at an O-O distance of 2.0 Å in the transition state), we found that the structure can relax to two alternate conformations for the oxygen adatoms: one involving both of them at Pt-Pt bridge sites along one edge of the triangular prism, and another where one of the oxygen atoms binds on top of a Pt corner site. It is slightly more probable for the system to relax towards the first conformation, since it is slightly more stable (and this is the one plotted in Fig. 12). Next, diffusion of the oxygen adatom towards the Pt corner site requires to overcome a barrier of 0.77 eV (labelled TS2 in Fig. 12). This movement of the oxygen atom to a Pt on-top location is necessary to activate it, making easier the subsequent reaction with CO (we have checked that the interaction between a bridging oxygen atom and CO leads to much larger barriers). The third barrier, involving the approach between CO and the O atom, is the highest one (0.85 eV) and becomes the rate-limiting step for the whole reaction pathway. As in the previous case, we also find a C-O distance of 2.0 Å at the transition state. The last stage, similarly to the previous case, requires a small barrier (0.14 eV) for the final desorption of CO_2. The comparison of Figs. 11 and 12 reveals that the barriers for the oxidation of CO are similar, so the reaction can take place starting from different initial configurations in which the CO and O_2 reactants are positioned nearby.

Next, we discuss the results for similar reaction pathways in the case of the $NbPt_{17}$ cluster. As in the case of Pt_{18}, we have considered two situations, with different initial conformations for co-adsorbed CO and O_2. In the first case (Fig. 13), CO is adsorbed as the conformer (b) in Fig. 5, and O_2 is later adsorbed next to CO, (the configuration shown in Fig. 10c), with an overall initial binding energy of 3.17 eV. As in the case of Pt_{18}, attempts of displacing CO towards an intact O_2 molecule result in quite high barriers of more than 1 eV, so again the initial reaction step must be the dissociation of O_2. Such dissociation takes place with a moderate barrier of 0.68 eV, with a O-O distance at the transition state of 2.1 Å. In the final intermediate state, one of the oxygen atoms relaxes to a Pt-Pt bridge position close to CO, sharing with it one Pt atom. That is, to react with CO, this oxygen adatom must diffuse to a neighbour Pt-Pt bridge site, from where it will finally form the new C-O bond. The activation energy for the CO bond formation is moderate (0.60 eV), and again a metastable CO_2 complex is formed, with sp^2 bonding and two bonds to Pt atoms. Final desorption of CO_2 is again easy, with a very small reaction barrier of only 0.15 eV.

The results for the second reaction pathway for CO_2 formation at $NbPt_{17}$ are shown in Fig. 14. Now we start from conformation (h) in Fig. 10, with O_2 initially adsorbed at its more stable location, and CO is also bonded at a quite stable site, in close proximity to O_2. In this case, O_2 dissociation takes place with a slightly lower barrier of 0.61 eV; interestingly, now the transition state is reached at a longer O-O distance of 2.5 Å. This is probably related to the fact that, at the TS, one of the oxygen atoms must pass on top of the Pt edge atom before reaching its final position on a hollow site between three Pt atoms (see inset TS1 in Fig. 14). From such hollow site, the oxygen adatom needs to be activated to a Pt-Pt bridge location in order to react with CO, with an associated barrier of 0.73 eV, the highest one along this reaction pathway. The final desorption of CO_2 requires again to break the O-Pt bond, a process mediated by a moderate barrier of 0.23 eV. Again the comparison of the two reaction paths of Figs. 13 and 14 reveals that the oxidation of CO can take place by starting from different $NbPt_{17}$ isomers and different configurations of the coadsorbed CO and O_2 species.

3.5. CO oxidation reaction at $MoPt_{17}$

After studying in detail the effects of the presence of a Nb impurity, we have performed similar simulations for a $MoPt_{17}$ cluster, that is, an 18-atoms cluster with a Mo impurity instead of Nb. Experiments by Ferrari et al. [26] indicate that the presence of Mo also produces a sizable reduction of the binding strength of CO to medium-sized Pt clusters. Since the presence of Mo apparently affects CO binding in a similar way as to the presence of Nb does, we have checked the effect of replacing the Nb impurity by Mo in the most relevant steps of the CO oxidation reaction.

In the first place, we have selected a few of the most stable conformations for $NbPt_{17}$, relaxing those structures after substituting the Nb impurity by a Mo one. The results, shown in Figure S7 of the suplementary material, demostrate that the replacement of Nb by Mo does not result in a significant change of the energy ordering of the confirmations studied; again, the two most stable isomers for $NbPt_{17}$ have almost identical energies in the $MoPt_{17}$ case. For that reason, we have again selected the same isomer as in the $NbPt_{17}$ case to study the coadsorption and reaction of CO and O_2.

Fig. 15 shows the binding energies of either CO or O_2 to the $MoPt_{17}$ cluster, at their most stable binding sites. Again, changing the dopant does not result in large changes of the relative energetic ordering between different conformations; however, there is a small general increase (of the orden of 0.1-0.2 eV) of the binding energies (both in the

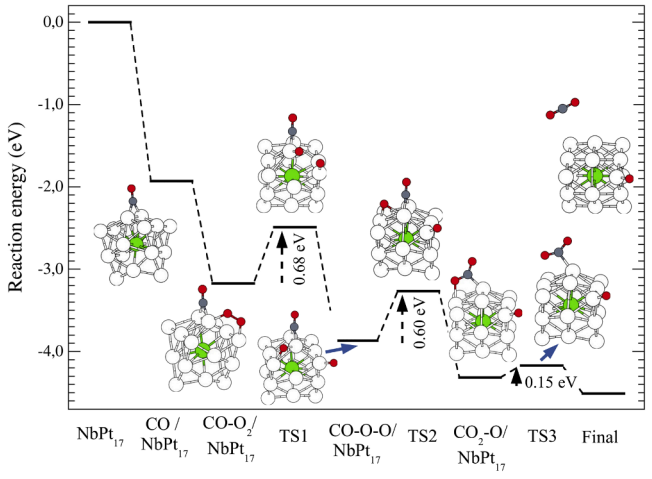

Fig. 13. Reaction energies and energy barriers for CO_2 formation at a $NbPt_{17}$ cluster (first pathway). Insets show the relaxed structures of all the intermediate and transition states.

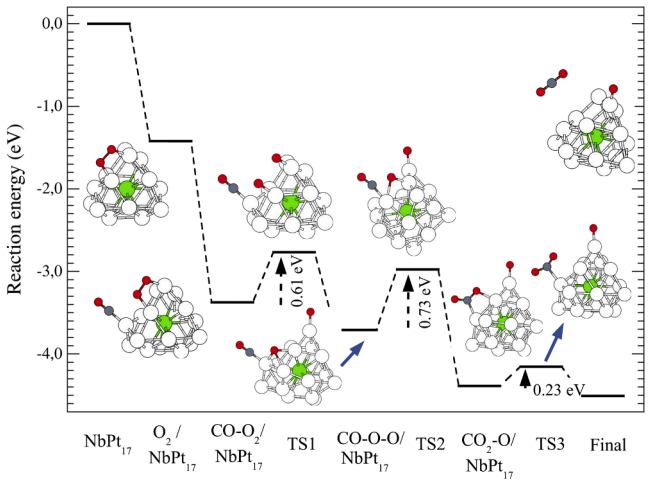

Fig. 14. Reaction energies and energy barriers for CO_2 formation at a $NbPt_{17}$ cluster (second pathway). Insets show the relaxed structures of all the intermediate and transition states.

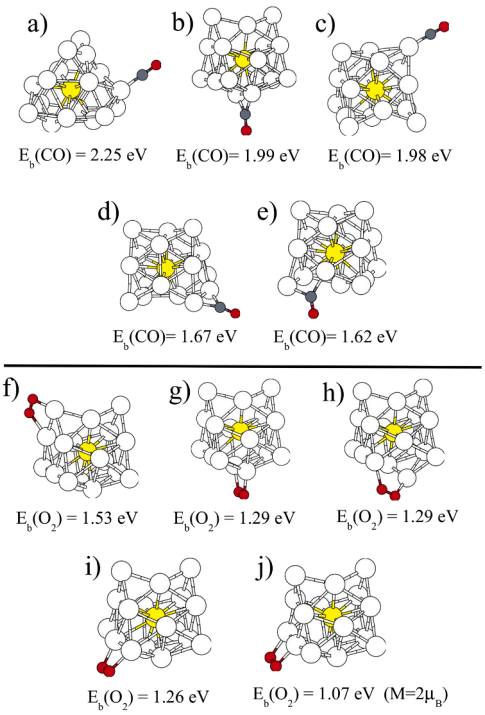

Fig. 15. Equilibrium structures and binding energies for adsorption of either CO (configurations a-e) or O_2 (configurations f-j) at a $MoPt_{17}$ cluster. Excepting structure (j), magnetic moments are always zero. The yellow sphere represents the Mo impurity. (For interpretation of the references to colour in this figure legend, the reader is referred to the web version of this article.)

CO case and in the O_2 case) for the $MoPt_{17}$ cluster. This means that doping with Mo results in a slightly larger cluster reactivity, as compared to the Nb case.

Then, we have performed aditional simulations of the coadsorption of CO and O_2 and their mutual reaction at the $Pt_{17}Mo$ cluster. To establish a more direct comparison with the $Pt_{17}Nb$ case, we have again reproduced the same reaction pathway reported in Fig. 14, which involves coadsorption of CO and O_2 at their most stable conformations, respectively. Overall, the results (shown in Fig. 16) are very similar to the ones obtained for $Pt_{17}Nb$. The main barriers (for O_2 dissociation and for the O-CO bond formation) are just a bit larger than the ones found in the $Pt_{17}Nb$ case. Such small increase is caused by the slightly stronger

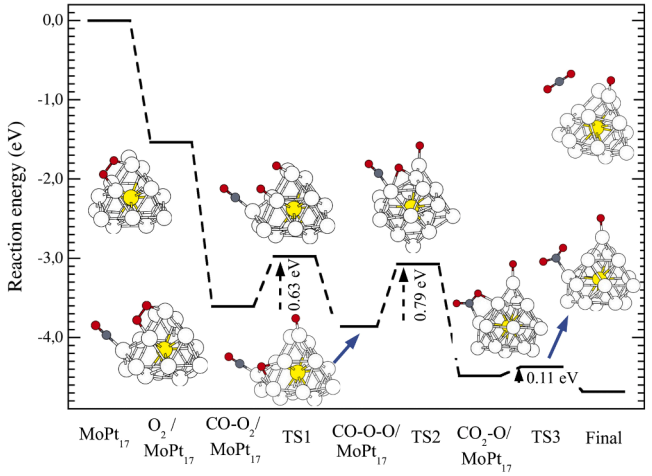

Fig. 16. Reaction energies and energy barriers for CO_2 formation at a $MoPt_{17}$ cluster. Insets show the relaxed structures of all the intermediate and transition states.

binding energies of both O_2 and CO.

4. Conclusions

In this manuscript, we have studied in detail the CO oxidation reaction at a Pt_{18} cluster and a Nb-doped $NbPt_{17}$ cluster. In the case of the pure Pt_{18} cluster, we found that the cluster structure can strongly influence the adsorption of carbon monoxide. The triangular prism conformation of the Pt_{18} ground state (much lower in energy than any other isomer) makes the cluster less reactive towards CO (by 0.3 eV, compared to a stacked square isomer). The high spin state of the triangular prism isomer, and also a small energy gap opening at the Fermi level, seem to be related to such smaller reactivity. Also, for both isomers, we found important variations of CO binding energy (up to 0.5 eV or more) at the different surface sites of the Pt_{18} cluster. The markedly lower binding energy of CO at other surface sites will result in a lower tendency of the cluster to be poisoned by CO. In the case of $NbPt_{17}$, the presence of the Nb atom at a central location produces a significant distortion of the triangular prism structure; also, the Nb atom transfer a sizable amount of charge to the surrounding Pt atoms. The combined result of these two effects is to raise the CO binding energy at the most stable site up to 2.05 eV, a value very similar to the one found for the Pt_{18} stacked square isomer. Besides, for the $NbPt_{17}$ cluster, we also found a sizable variability of the CO binding energy around the cluster surface, with values as low as 1.2-1.3 eV.

Molecular O_2 is quite strongly adsorbed on either Pt_{18} or $NbPt_{17}$, with an adsorption energy at the most stable binding sites of the order of 1.5 eV. Interestingly, adsorption is slightly more stable at the pure Pt_{18} cluster, meaning that the reduced reactivity of this cluster only affects CO adsorption. As it happened for CO, the O_2 binding energies vary a lot by placing the molecule on other Pt surface sites, and they can decrease up to values of around 0.6-0.7 eV.

Since the O_2 binding energy is only slightly smaller than the CO binding energy, it is reasonable to conclude that under standard reaction conditions both Pt_{18} and $NbPt_{17}$ clusters will not be completely poisoned by CO, and co-adsorption of both CO and O_2 adsorbates will easily take place. In some cases, we have even found weak cooperative effects which favour coadsorption at neightbouring sites. After coadsorption, for both pure and doped clusters formation of CO_2 requires to overcome several moderate activation barriers, with the highest ones being of the order of 0.7-0.8 eV. In all cases studied, it is necessary to first dissociate the O_2 molecule, prior to the formation of the C-O bond in CO_2. In this respect, our results differ from the ones obtained by Lian et al. [44] for very small mixed Pt_3M clusters, where is was found that direct reaction between CO and intact O_2 was preferred. Finally, for both Pt_{18} and $NbPt_{17}$ the final reaction step involves desorption of a CO_2 complex bonded to two Pt atoms, with the C atom showing sp^2-type bonding; this step proceeds easily in all cases, with small barriers of 0.25 eV or less.

Overall, the results show that in both pure and Nb-doped Pt_N clusters of medium size, CO_2 can be readily produced at these catalysts. Initial binding of CO seems to be influenced by structural effects (we found that the very stable shape of pure Pt_{18} reduces CO adsorption energy), and doping by Nb has the main effect of causing very important deformations to the cluster. Also, it was found that the presence of the Nb dopant has the additional effect of completely removing the magnetization of the platinum cluster. Finally, the comparison of the results obtained for $NbPt_{17}$ and for $MoPt_{17}$ demonstrates that the presence of a Mo impurity instead of a Nb one causes similar modifications to the structure and reactivity of the pure Pt cluster. The only noticeable difference between the two dopants is a very small enhancement of the reactivity towards CO and O_2 binding in the Mo case, with changes in binding energies of approximately 0.1-0.2 eV.

CRediT authorship contribution statement

L.M. Molina: Conceptualization, Methodology, Software,

Validation, Formal analysis, Investigation, Data curation, Visualization, Writing – original draft, Writing – review & editing. **C. Arranz-Simón:** Conceptualization, Methodology, Software, Formal analysis, Investigation, Data curation, Visualization. **J.A. Alonso:** Conceptualization, Methodology, Formal analysis, Investigation, Writing – original draft, Writing – review & editing, Funding acquisition, Project administration, Supervision.

Declaration of Competing Interest

The authors declare that they have no known competing financial interests or personal relationships that could have appeared to influence the work reported in this paper.

Acknowledgments

Work supported by Ministerio de Ciencia e Innovación of Spain (Grant PID2019-104924RB-I00 funded by MCIN/AEI/10.13039/501100011033) and University of Valladolid (GIR Nanostructure Physics).

Supplementary material

Supplementary material associated with this article can be found, in the online version, at doi:10.1016/j.mcat.2022.112749.

References

[1] M.K. Debe, Nature 486 (2012) 43–51.
[2] O.T. Holton, J.W. Stevenson, Platinum Met. Rev. 57 (2013) 259.
[3] A.A.J. Parker, G. Opletal, A.S. Barnard, J. Appl. Phys. 128 (2020) 014301.
[4] H. Kazutaka, S. Shoichiro, Bull. Chem. Soc. Jpn. 82 (2009) 1299–1303.
[5] R.A. Periana, D.J. Taube, S. Gamble, H. Taube, T. Satoh, H. Fujii, Science 280 (1998) 560–564.
[6] M. Shao, A. Peles, K. Shoemaker, Nano Lett. 11 (2011) 3714.
[7] T. Imaoka, H. Kitazawa, W.-J. Chun, S. Omura, K. Albrecht, K. Yamamoto, J. Am. Chem. Soc. 135 (2013) 13089.
[8] T. Jacob, Fuel Cells 6 (2006) 159–181.
[9] H. Yano, J. Inukai, H. Uchida, M. Watanabe, P.K. Babu, T. Kobayashi, J.H. Chung, E. Oldfield, A. Wieckowski, Phys. Chem. Chem. Phys. 8 (2006) 4932.
[10] S. Vajda, M.J. Pellin, J.P. Greeley, C.L. Marshall, L.A. Curtiss, G.A. Ballentine, J. W. Elam, S. Catillon-Mucherie, P.C. Redfern, F. Mehmood, P. Zapol, Nat. Mater. 8 (2009) 213.
[11] P.L. Rodríguez-Kessler, A.R. Rodríguez-Domínguez, J. Chem. Phys. 143 (2015) 184312.
[12] H. Choi, S. Oh, J.Y. Park, Catal. Today 352 (2020) 212–219.
[13] C. Cui, Z. Luo, J. Yao, CCS Chem. 1 (2019) 215225.
[14] J. Russell, P. Zapol, P. Král, L.A. Curtiss, Chem. Phys. Lett. 536 (2012) 9–13.
[15] Z.-P. Liu, P. Hu, A. Alavi, J. Am. Chem. Soc. 124 (2002) 14770–14779.
[16] S. Lin, X. Ye, R.S. Johnson, H. Guo, J. Phys. Chem. C 117 (2013) 17319–17326.
[17] M.-a. Yu, Y. Feng, L. Gao, S. Lin, Phys. Chem. Chem. Phys. 20 (2018) 20661–20668.
[18] V. Kumar, Y. Kawazoe, Phys. Rev. B 77 (2008), 205418.
[19] H.K. Yuan, H. Chen, A.L. Kuang, B. Wu, J. Mag. Mag. Mater. 331 (2013) 7–16.
[20] L. Li, A.H. Larsen, N.A. Romero, V.A. Morozov, C. Glinsvad, F. Abild-Pedersen, J. Greeley, K.W. Jacobsen, J.K. Nørskov, J. Phys. Chem. Lett. 4 (2013) 222–226.
[21] Y.-H. Chin, C. Buda, M. Neurock, E. Iglesia, J. Am. Chem. Soc. 133 (2011) 15958–15978.
[22] D.A. Esan, M. Trenary, J. Chem. Phys. 154 (2021) 114701.
[23] J. Baschuk, X. Li, Int. J. Energy Res. 25 (2001) 695.
[24] S. Ehteshamia, S. Chan, Electrochim. Acta 93 (2013) 334–345.
[25] T. Rocha, F. Ibanhi, F. Colmati, J. Linares, V. Paganin, E. Gonzalez, J. Appl. Electrochem. 43 (2013) 817–827.
[26] P. Ferrari, L.M. Molina, V.E. Kaydashev, J.A. Alonso, P. Lievens, E. Janssens, Angew. Chem. Int. Ed. 55 (2016) 11059–11063.
[27] P. Ferrari, G. Libeert, N.M. Tam, E. Janssens, Cryst. Eng. Comm. 22 (2020) 4807–4815.
[28] A. Ugartemendia, K. Peeters, P. Ferrari, A. de Cozar, J.M. Mercero, E. Janssens, E. Jimenez-Izal, ChemPhysChem. 22 (2021) 1603–1610.
[29] L. Li, et al., J. Phys. Chem. C 125 (2021) 13780–13787.
[30] S. Nigam, C. Majumder, Appl. Surf. Sci. 547 (2021) 149160.
[31] S. Lee, C. Fan, T. Wu, S.L. Anderson, J. Am. Chem. Soc. 126 (2004) 5682–5683.
[32] B. Yoon, H. Häkkinen, U. Landman, A.S. Wörz, J.-M. Antonietti, S. Abbet, K. Judai, U. Heiz, Science 307 (2005) 403–407.
[33] J.S. Spendelow, J.D. Goodpaster, P.J.A. Kenis, A. Wieckowski, J. Phys. Chem. B 110 (2006) 9545–9555.
[34] S.M. McClure, D.W. Goodman, Chem. Phys. Lett. 469 (2009) 1–13.
[35] M.A. van Spronsen, J.W.M. Frenken, I.M.N. Groot, Chem. Soc. Rev. 46 (2017) 4347–4374.
[36] A. Alavi, P. Hu, T. Deutsch, P.L. Silvestrelli, J. Hutter, Phys. Rev. Lett. 80 (1998) 3650.
[37] U. Heiz, A. Sanchez, S. Abbet, W.D. Schneider, J. Am. Chem. Soc. 121 (1999) 3214–3217.
[38] A. Beniya, S. Higashi, N. Ohba, R. Jinnouchi, H. Hirata, Y. Watanabe, Nat. Commun. 11 (2020) 1888.
[39] S.B. Vendelbo, C.F. Elkjær, H. Falsig, I. Puspitasari, P. Dona, L. Mele, B. Morana, B. J. Nelissen, R. van Rijn, J.F. Creemer, P.J. Kooyman, S. Helveg, Nat. Mater. 13 (2014) 884–890.
[40] B. Demirdjian, I. Ozerov, F. Bedu, A. Ranguis, C.R. Henry, ACS Omega 6 (2021) 13398–13405.
[41] V. Klimavicius, S. Neumann, S. Kunz, T. Gutmann, Catal. Sci. Technol. 9 (2019) 3743–3752.
[42] R. Vakili, E.K. Gibson, S. Chansai, S. Xu, N. Al-Janabi, P.P. Wells, C. Hardacre, A. Walton, X. Fan, Chem. Cat. Chem. 10 (2018) 4238–4242.
[43] Y. Feng, Q. Wan, H. Xiong, S. Zhou, X. Chen, X.I. Pereira-Hernandez, Y. Wang, S. Lin, A.K. Datye, H. Guo, J. Phys. Chem. C 122 (2018) 22460–22468.
[44] X. Lian, W. Guo, F. Liu, Y. Yang, P. Xiao, Y. Zhang, W. Tian, Comput. Mater. Sci. 96 (2015) 237–245.
[45] H. Xu, M. Zhang, Y. Chen, H. Liu, K. Xu, X. Huang, Comput. Theor. Chem. 1061 (2015) 52–59.
[46] G. Ramos-Sánchez, P.B. Balbuena, J. Electroanal. Chem. 716 (2014) 23–30.
[47] J. Xu, Y. Wang, J. Lu, X. Li, X. Wang, J. Yang, Vacuum 183 (2021) 109847.
[48] Y. Xu, W.A. Shelton, W.F. Schneider, J. Phys. Chem. A 110 (2006) 5839–5846.
[49] Y. Xu, R.B. Getman, W.A. Shelton, W.F. Schneider, Phys. Chem. Chem. Phys. 10 (2008) 6009–6018.
[50] S. Dobrin, Phys. Chem. Chem. Phys. 14 (2012) 12122–12129.
[51] J.J. Mortensen, L.B. Hansen, K.W. Jacobsen, Phys. Rev. B 71 (2005) 035109.
[52] J. Enkovaara, C. Rostgaard, J.J. Mortensen, J. Chen, M. Dulak, L. Ferrighi, J. Gavnholt, C. Glinsvad, V. Haikola, H.A. Hansen, H.H. Kristoffersen, M. Kuisma, A.H. Larsen, L. Lehtovaara, M. Ljungberg, O. Lopez-Acevedo, P.G. Moses, J. Ojanen, T. Olsen, V. Petzold, N.A. Romero, J. Stausholm-Møller, M. Strange, G. A. Tritsaris, M. Vanin, M. Walter, B. Hammer, H. Häkkinen, G.K.H. Madsen, R. M. Nieminen, J.K. Nørskov, M. Puska, T.T. Rantala, J. Schiøtz, K.S. Thygesen, K. W. Jacobsen, J. Phys. Condens. Matter 22 (2010) 253202.
[53] J.P. Perdew, K. Burke, M. Ernzerhof, Phys. Rev. Lett. 77 (1996) 3865.
[54] M.A.L. Marques, M.J.T. Oliveira, T. Burnus, Comput. Phys. Commun. 183 (2012) 2272.
[55] D.C. Liu, J. Nocedal, Math. Program. 45 (1989) 503.
[56] J.-Y. Chung, F. Aksoy, M.E. Grass, H. Kondoh, P. Ross Jr., Z. Liu, B.S. Mun, Surf. Sci. 603 (2009).L35-L38
[57] F. Gao, Y. Wang, Y. Cai, D.W. Goodman, J. Phys. Chem. C 113 (2009) 174–181.
[58] X. Su, P.S. Cremer, Y.R. Shen, G.A. Somorjai, J. Am. Chem. Soc. 119 (1997) 3994–4000.
[59] G. Rupprechter, T. Dellwig, H. Unterhalt, H.J. Freund, J. Phys. Chem. B 105 (2001) 3797–3802.
[60] R.F.W. Bader, Atoms in molecules: A quantum theory, Oxford University Press, New York, 1990.
[61] R. Wang, L. Zhao, J. Jia, H.S. Wu, AIP Adv. 8 (2018) 035307.
[62] L.M. Molina, B. Hammer, J. Chem. Phys. 123 (2005) 161104.
[63] D. Tang, C. Hu, J. Phys. Chem. Lett. 2 (2011) 2972–2977.
[64] L.M. Molina, A. Lesarri, J.A. Alonso, Chem. Phys. Lett. 468 (2009) 201–204.